Macromolecules

Article

Cite This: Macromolecules 2018, 51, 5294−5303

Multistimuli-Responsive Intrinsic Self-Healing Epoxy Resin Constructed by Host−Guest Interactions

Zhen Hu,[*,†] Dayu Zhang,[†] Fei Lu,[†] Weihao Yuan,[†] Xirong Xu,[†] Qian Zhang,[†] Hu Liu,[‡,§] Qian Shao,[∥] Zhanhu Guo,[*,§] and Yudong Huang[*,†]

[†]School of Chemistry and Chemical Engineering, MIIT Key Laboratory of Critical Materials Technology for New Energy Conversion and Storage, Harbin Institute of Technology, Harbin 150001, China

[‡]National Engineering Research Center for Advanced Polymer Processing Technology, Zhengzhou University, Zhengzhou 450002, China

[§]Integrated Composites Laboratory (ICL), Department of Chemical & Biomolecular Engineering, University of Tennessee, Knoxville, Tennessee 37996, United States

[∥]College of Chemical and Environmental Engineering, Shandong University of Science and Technology, Qingdao 266590, China

Supporting Information

ABSTRACT: The self-healing abilities inside polymeric materials are desirable functions in materials science. Host−guest chemistry, combined with excellent properties of graphene, was used for the construction of multistimuli-responsive intrinsic self-healing epoxy materials. By ultraviolet (UV) curing, the unsaturated epoxy resin was connected with β-cyclodextrin/graphene complex through free radical copolymerization. The introduced complex, acting as macro-cross-linker and photothermal agent, can reconnect the damage-induced broken bonds through dynamic host−guest interaction. In this work, the epoxy composites exhibited a high healing efficiency of up to 79.2% and tensile strength of up to 20.8 MPa under heating or near-infrared stimulation, which represent relatively excellent values among all the reported intrinsic self-healing epoxy resin and host−guest self-healing systems.

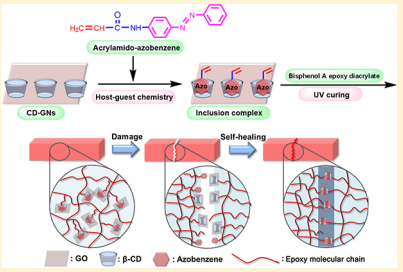

1. INTRODUCTION

Inspired by natural creatures, the concept of self-healing materials has been explored and has obtained huge developments in recent years.[1−5] Epoxy resins are important polymeric materials applied in many fields, including advanced composites, coatings, adhesives, and printed circuit boards. However, the brittle nature of epoxy resins makes it easy to form micrometer damages during service. These micrometer cracks may gradually develop into fatal damage and cause failure of the whole materials. To settle this issue, several strategies have been explored for the spontaneous healing of epoxy resins to recover these mechanical damages.

Generally speaking, the healing processes could be divided into two categories: extrinsic or intrinsic. The extrinsic strategy pre-embeds microcapsules[6−10] or vascular systems[11,12] into the resin. Upon cracking damage, the healing agents can be released to recover the defect. However, the microcapsules can heal the resin for only once, while the vascular systems are too complex to produce in industrial scale. Alternatively, intrinsic self-healing can be realized by introducing reversible dynamic bonds to the epoxy resins. Under external stimuli, the reversible bond can unlock/lock the cross-linking structure to self-heal the resins. The typical dynamic bonds responsible for intrinsic self-healing include Diels−Alder bond,[13−18] disulfide exchange,[19−21] and ester exchange.[22−24]

Noncovalent chemistry, such as hydrogen bonding,[25−27] π−π stacking,[28,29] and metal−ion binding,[30,31] is another strategy to develop intrinsic self-healing materials. Host−guest chemistry, one of the most important noncovalent effects, has become a powerful approach to design self-healing materials in recent years. Owing to their hydrophilicity, biocompatibility, low cost, and ease of chemical modification, cyclodextrins (CDs) are considered to be the most potential candidate for the construction of self-healing materials. CDs can form host−guest recognition with specific guest groups (azobenzene, adamantane, ferrocene, etc.) with high selectivity and reversible noncovalent interactions. While the dynamic bond based self-healing system has a relatively low healing efficiency and usually requires external energy stimulus, the CDs based host−guest interactions often lead to rapid and high efficiency of self-healing. For example, Harada's group has reported a pioneering work on the preparation of self-healing poly(acrylic acid) hydrogel due to reversible multipoint cross-links between β-CD and ferrocene.[32] Inspired by this work, more self-healing polymer architectures are developed based on host−guest recognition between ferrocene and CDs, including poly(ethylene glycol),[33] polyethylenimine,[34] and poly(glycidyl

Received: May 28, 2018
Revised: June 27, 2018
Published: July 11, 2018

DOI: 10.1021/acs.macromol.8b01124
Macromolecules 2018, 51, 5294−5303

methacrylate).[35] Furthermore, other potential guest molecules are investigated to form host−guest complex with CDs (such as adamantane,[36−39] imidazole,[40] and phenolphthalein[41]), which constructs more CDs based self-healing materials. Efforts may be focused on improving the mechanical strength and exploring more types of guest molecules to meet the requirement of practical applications.

In this paper, emphasis is put on solving the aforementioned problems by using the host−guest interactions between β-CD and azobenzene.[42,43] Previous studies have revealed that the association constant (K_a) has a great impact on the efficiency of self-healing, and a larger K_a usually leads to a better healing effects. Owing to the K_a of β-CD with azobenzene is ∼10 000 M^{-1},[44] the combination of β-CD/azobenzene is quite suitable for fabricating the self-healing system.[45] In the present study, epoxy resins based on reversible host−guest network are prepared. Acrylamido azobenzene moieties, regarding as guest component, can be introduced into the epoxy acrylate network via copolymerization. On the other hand, the cyclodextrin moieties in β-CD/graphene can incorporate azobenzene moieties in epoxy and act as noncovalent macrolinkers. The interactions between β-CD and azobenzene, as a controller to unlock or lock the connecting of epoxy network and graphene, endowed the resins with intrinsic self-healing ability and excellent mechanical property.

2. EXPERIMENTAL SECTION

2.1. Materials. The β-cyclodextrin, *p*-toluenesulfonyl chloride, and ammonium chloride were supplied by Energy Chemical Technology Co., Ltd. Graphite powders (purity of >99.95% metal basis), *p*-aminoazobenzene, triethylamine, hydroquinone, acryloyl chloride, butyl acrylate, *N*,*N*-dimethylformamide, dicyclohexylcarbodiimide, and other common reagents were supplied by Aladdin Reagent Co., Ltd. Bisphenol A epoxy diacrylate (molecular weight of 452, viscosity of 15 000−25 000 mPa·s, acid value of ≤8 mg KOH/g) and 1-hydroxycyclohexyl phenyl ketone (excitation wavelength of ∼330 nm) were purchased from Guangzhou Lihou Trade Co., Ltd.

2.2. Synthesis of Acrylamidoazobenzene (AAAB). *p*-Aminoazobenzene (1.97 g), triethylamine (TEA), and a small amount of hydroquinone were dissolved in 20 mL of benzene successively. Then, 0.8 mL of acryloyl chloride was slowly added at room temperature. The above solution was reflux reacted for 3 h at 60 °C to generate a red-orange solid. The obtained solution was then processed by cooling down, filtering, and drying. The red-orange powder was collected, washed by distilled water, and recrystallized in ethanol twice. The AAAB crystal was ultimately obtained. Yield: 56.3%. IR: 3280, 3200, 3135, 3070, 1670, 1600, 1555, and 985 cm^{-1}. ^{1}H NMR (400 MHz, $CDCl_3$, δ): 5.81−6.32 (H of −CH═$\underline{CH_2}$), 6.50 (H of −$\underline{CH}$═CH_2), 7.51, 7.75, 7.96 (H of benzene rings) ppm. ^{13}C NMR (400 MHz, $CDCl_3$, δ): 163.6 (C of −NH−($\underline{C}$═O)−CH═CH_2), 152.6, 149.2 (C of benzene rings connected with −N═N−), 140.3 (C of benzene rings connected with amide group), 130.9, 129.1, 124.1, 122.8 (other C of benzene rings), 128.6 (C of −$\underline{CH}$═CH_2), 120.1 (C of −CH═$\underline{CH_2}$) ppm. MS *m*/*z*: (positive ion ESI) 252.31 for $[M + H]^+$. The characterization spectra are shown in Figure S1.

2.3. Preparation of Mono-6-deoxy-6-amino-β-cyclodextrin (6-NH_2-β-CD). β-CD (50 g) was dispersed into 1.2 L of deionized water under stirring. Then, 13.0 g of *p*-toluenesulfonyl chloride (*p*-TsCl) was added into the system slowly to make the substitution to occur at the C6 position. The mixture was reacted overnight with intense agitation. Then, 200 mL of sodium hydroxide (20 g) aqueous solution was added dropwise slowly. The resultant solution was filtered to remove unreacted *p*-TsCl. Then, ammonium chloride (60.0 g) was added until the mixture was acidized to pH = 8 to terminate the reaction. The final solution was cooled and kept in ice bath for 12 h. The raw product was obtained by suction filtration. The white precipitate (6-OTs-β-CD) was further purified by recrystallization from deionized water at least three times. Yield: 31.2%. IR: 3371, 2925, 1648, 1362, 1155, 1030, 830, and 580 cm^{-1}. ^{1}H NMR (400 MHz, DMSO-d_6, δ): 7.74, 7.44 (H of Ts benzene), 5.67 (OH-2 and OH-3 of β-CD), 4.77, 4.84 (H-1 of β-CD), 4.40−4.47 (OH-6 of β-CD), 3.31−3.66 (H-2, H-3, H-4, H-5, H-6 of β-CD), 2.44 (H of Ts methyl) ppm. ^{13}C NMR (400 MHz, DMSO-d_6, δ): 145.3, 133.1, 130.4, 128.1 (C of Ts benzene), 102.4 (C-1 of β-CD), 82.0 (C-4 of β-CD), 73.5 (C-3 of β-CD), 72.5 (C-2 of β-CD), 69.4 (C-5 of β-CD), 60.4 (C-6 of β-CD), 21.68 (C of Ts methyl) ppm. MS *m*/*z*: (positive ion ESI) 1289.76 for $[M + H]^+$. The characterization spectra are shown in Figure S2.

Powdered 6-OTs-β-CD was dissolved in a substantial excess of ammonia at 75 °C and stirred for 4 h. Then, a certain amount of acetone was added into the reaction at room temperature to get white precipitate. This raw product was dissolved in a mixed solution of CH_3OH/H_2O (v/v = 1:3) and precipitated by acetone for several times to remove the unreacted ammonia and 6-OTs-β-CD. The final product was dried at 50 °C in a vacuum for 24 h to obtain 6-NH_2-β-CD. Yield: 34.1%. IR: 3371, 2925, 1648, 1155, 1030, 850, 709, and 580 cm^{-1}. ^{1}H NMR (400 MHz, DMSO-d_6, δ): 5.64−5.68 (OH-2 and OH-3 of β-CD), 4.83 (H-1 of β-CD), 4.40 (OH-6 of β-CD), 3.30−3.66 (H-2, H-3, H-4, H-5, H-6 of β-CD) ppm. ^{13}C NMR (400 MHz, DMSO-d_6, δ): 102.4 (C-1 of β-CD), 82.0 (C-4 of β-CD), 73.5 (C-3 of β-CD), 72.5 (C-2 of β-CD), 60.4 (C-6 of β-CD) ppm. MS *m*/*z*: (positive ion ESI) 1134.52 for $[M + H]^+$. The characterization spectra are shown in Figure S3.

2.4. Preparation of β-CD-Graphene Nanosheets (CD-GNs). The improved Hummers method was applied to prepare graphene oxide (GO) by using high purity graphite powder as starting material. Briefly, GO (400 mg) and 6-NH_2-β-CD (250 mg, 0.22 mmol) were dissolved in 50 mL of anhydrous dimethylformamide (DMF). Subsequently, the mixture was reacted for 48 h with stirring in the presence of DCC (227 mg, 1.10 mmol). The insoluble impurity could be easily separated by filtration. The following high-speed centrifugation (12 000 rpm) removed most of the soluble impurity in DMF and gave CD-GNs precipitate with fairly high purity. In order to further purify the CD-GNs, the obtained precipitate was washed with H_2O for several times to remove unreacted 6-NH_2-β-CD. After drying under vacuum, gray solid powder CD-GNs was obtained.

2.5. Fabricating of CD-GNs/Epoxy Composite Films. A mixed solution consisting of CD-GNs (500 mg) and AAAB (45.56 mg) in THF (100 mL) was reacted for 24 h under stirring and refluxing in dark. Then, the solution was centrifuged at 12 000 rpm to get a black solid. The precipitate was washed with THF for several times to remove unconjugated CD-GNs and AAAB. The final product was dried under vacuum to give the CD-GNs/AAAB complex.

A certain amount of CD-GNs/AAAB complex and butyl acrylate (2.247 mL) was mixed in epoxy acrylate (2.5 g). The mixture was dispersed with the assistance of ultrasonic treatment for 10 min. After the addition of 1-hydroxycyclohexyl phenyl ketone (250 mg), the mixture solution was treated with ultrasonic for another 5 min. The CD-GNs/epoxy composite films were blade-casted with automatic film coater and then cured for 20 min with portable UV irradiation at room temperature.

2.6. Characterizations of Materials. Fourier transform infrared spectra (FT-IR, Bruker, Tensor 27), ^{1}H and ^{13}C NMR (Bruker, AVF400, 400 MHz), Raman spectra (Horiba Jobin Yvon, France), and XPS (RBD upgraded PHI-5000C ESCA system, Lemanse Elmer) were used to characterize the chemical structure of organic compounds and polymers. An atomic force microscope (AFM, Sounding Housing SPA 400) and a transmission electron microscope (TEM, JEOL, JEM-2100F) were used to investigate the microstate of the modified graphene. TGA tests were carried out with a thermogravimetric analyzer (Netzsch STA449C) from 20 to 850 °C in air at a heating rate of 10 °C/min. Dynamic mechanical analysis (DMA) was performed with a 01Db-metravib-DMA25 apparatus under the N_2 using tensile mode.

A razor blade was used to cut the samples into two pieces. Prior to the self-healing process, the damaged samples were irradiated by 365 nm UV light to disconnect the connection between the host and guest

DOI: 10.1021/acs.macromol.8b01124
Macromolecules 2018, 51, 5294−5303

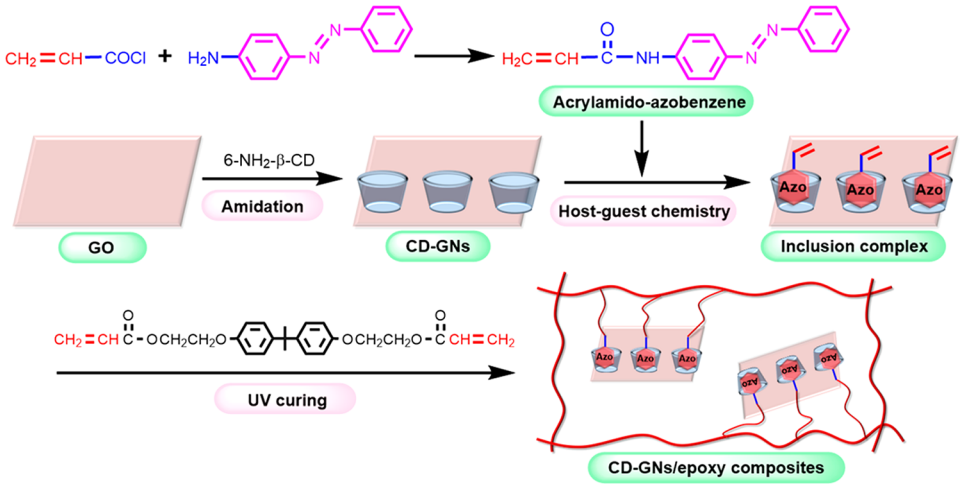

Figure 1. Preparation of CD-GNs/epoxy self-healing composites.

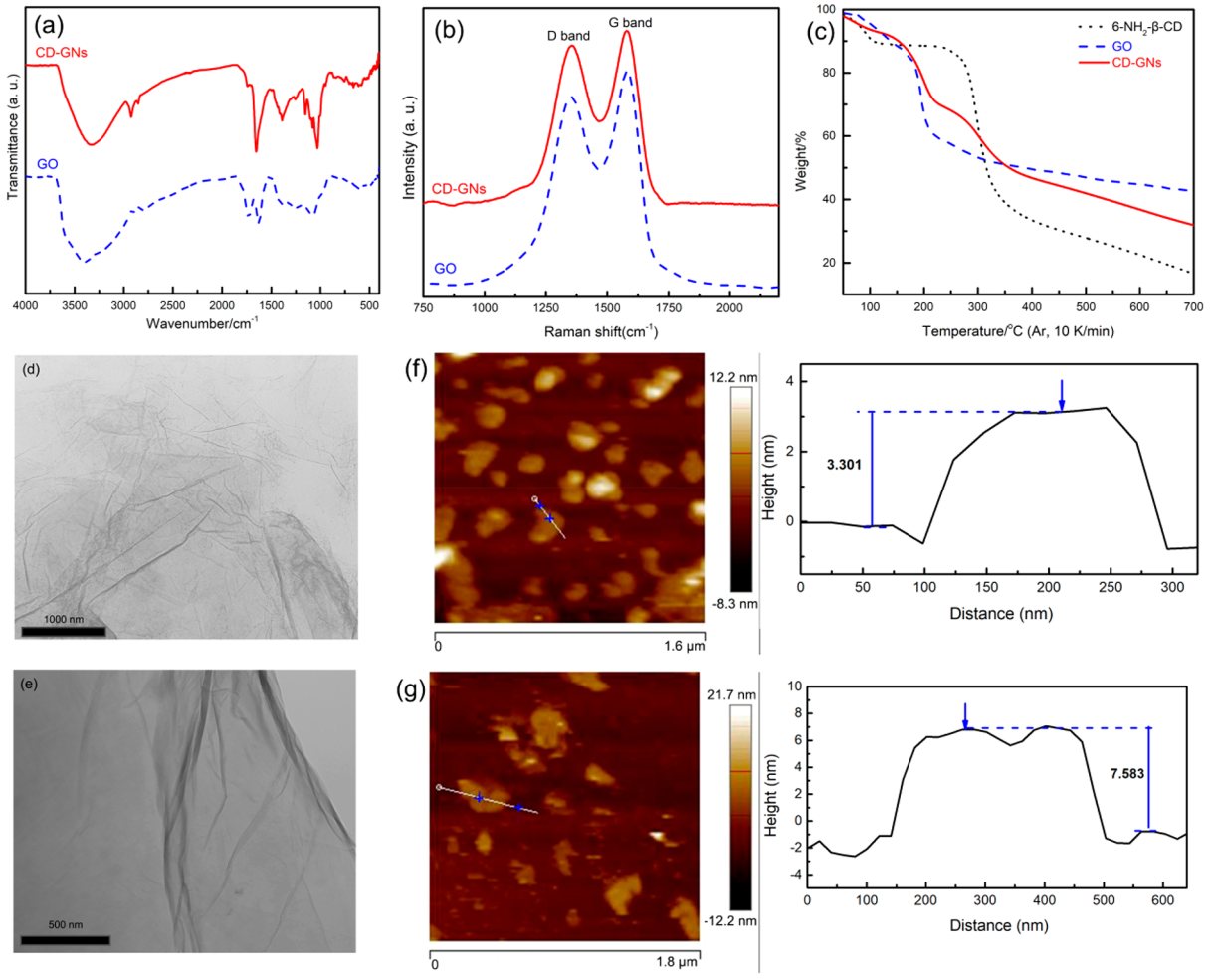

Figure 2. (a) FT-IR spectra, (b) Raman spectra, and (c) TGA curves of GO and CD-GNs; representative TEM images of (d) GO and (e) CD-GNs; AFM images of (f) GO and (g) CD-GNs with a height profile diagram.

molecules. Self-healing was processed by putting two pieces back together at 120 °C in dark to trigger the host−guest interactions. For photothermally triggered self-healing, the damage sites were irradiated by a NIR laser (LSR638CPX 5000 mW, Lasever) vertically. A thermal infrared imaging FLTR T460 was used to detect the temperature variation of the crack surface. The optical microscopy images of the cracks were taken with an optical microscope (Meiji Techno Co., Ltd., Japan) equipped with a digital camera. The mechanical properties of the films were measured on an Instron Universal Testing Machine (Model 4302, Instron Engineering Corporation) at a cross-head speed of 1 mm/min.

3. RESULTS AND DISCUSSION

UV-curing technology, owing to its environmental protection and energy saving, has been developed rapidly in many fields.

DOI: 10.1021/acs.macromol.8b01124
Macromolecules 2018, 51, 5294−5303

The light-triggered curing avoids the defect caused by thermal effects and has been extensively used in epoxy resin industry. In the present study, a novel UV-curable self-healing epoxy resin is designed by combining the self-healing concept and UV-curing technology. The synthetic route of the self-healing epoxy resin is shown in Figure 1. The CD-GNs/AAAB complex, acting as macro-cross-linker, is prepared by attaching the β-CD to graphene via amidation, followed by the inclusion of AAAB through host−guest interactions. The above CD-GNs/AAAB is readily blended with unsaturated epoxy resin via a facile UV-curing process to fabricate epoxy composite films.

β-CD and azobenzene, known as one of the most representative host−guest pairs, can form stable inclusion complexes with high association constant. However, the azobenzene is rarely reported to be used as guest molecules in the self-healing system.[45] In the present study, acrylic acid monomer was modified with aminoazobenzene to synthesize the guest monomer. The detailed characterization of the AAAB is shown in Figure S1 (Supporting Information). Graphene is selected as versatile fillers providing heat or photothermally triggered self-healing to the resin.[46,47] In order to effectively introduce the graphene into epoxy resin, the surface of graphene was decorated by β-CD using amidation, resulting in a CD-GNs nanohybrid. The decorated 6-NH_2-β-CD was synthesized in our lab. The detailed characterization of the modified β-CD is shown in Figures S2 and S3. Because of its ultrahigh specific surface area, ease of functionalization, and excellent photothermal activity, graphene is considered to be an outstanding photothermal agent.[48−50] Compared to heat, light stimuli are easily achievable, inexpensive, and controllable. Owing to the high efficiency photothermal conversion of CD-GNs and the accurate location of the NIR laser, photothermally triggered self-healing could be easily achieved with no obvious negative effects on the unirradiated area.

The functional groups of the β-CD decorated graphene were characterized by FT-IR spectroscopy. Figure 2a shows the characteristic peaks of GO located at ~3411 cm^{-1} (O−H), 2916 cm^{-1} (C−H), 1727 cm^{-1} (C═O), 1628 cm^{-1} (O−H bending vibration), and 1074 cm^{-1} (epoxy groups).[51] The IR spectrum of CD-GNs represents several new characteristic peaks at around ~1384 cm^{-1} (O−H bending vibration of β-CD), 1655 cm^{-1} (the C═O absorption of amide), and 1027 cm^{-1} (C−O absorption of β-CD), indicating the decorating of β-CD on GO.[52] The surface chemical state of modified graphene is examined by XPS (Figure S4). Quantitative analysis shows that the N element in the CD-GNs is increased from 0 to 1.30%, indicating the introduction of amide groups. The high-resolution C 1s spectra of CD-GNs also reveal a reduction of carboxyl content due to the amidation, which can be an evidence for the β-CD attaching. Both the Raman spectra of GO and CD-GNs (Figure 2b) show the characteristic G (intense tangential mode, 1350 cm^{-1}) and D bands (disordered induced peak, 1580 cm^{-1}), respectively. After GO is modified by β-CD, a larger I_D/I_G (0.94) is observed compared to that of GO (0.86). This change is attributed to more defects and higher degree of disorders that are introduced into graphene during amidation,[53,54] further confirming the successful attachment of β-CD. Moreover, the content of β-CD in the CD-GNs nanohybrid is calculated by TGA (Figure 2c). CD-GNs represents a progressive weight loss beginning at ~150 °C, and 31.86% mass residue is observed at 700 °C, which can be attributed to the pyrolysis of the oxygen-containing groups and β-CD.[55,56] By considering the mass residues of GO (42.60%) and 6-NH_2-β-CD (16.57%), the amount of attached β-CD molecules is calculated to be 41.3 wt % (3.64×10^{-4} mol g^{-1} CD-GNs), indicating that plenty of β-CD molecules are anchored onto graphene.

The morphology of CD-GNs is detected by TEM and AFM. The TEM images of both GO and CD-GNs demonstrate the lamella structure of graphene (Figures 2d and 2e). While the ultrathin property of GO causes a wrinkled topology, the CD-GNs represent a thicker morphology due to the decoration of β-CD. It can be known from AFM that the average thickness of CD-GNs (7.58 nm) is much greater than that of GO sheets (3.30 nm) (Figures 2f and 2g). The greater thickness of CD-GNs can be attributed to the anchorage of β-CD molecules on the graphene lamellar structure. It is shown that the GO and CD-GNs represent excellent dispersion in various solvents (such as water, ethanol, DMF, THF, etc.). Because of the functional groups and hydrophilicity of β-CD, CD-GNs show a better dispersion than GO. In particular, the solution of CD-GNs is stable and few precipitates are formed after 3 weeks storage (Figure S5). Moreover, the CD-GNs solution also possesses excellent dispersibility after several hours NIR or UV light irradiation.

Based on molecular design, β-CD modified graphene was obtained. Subsequently, the CD-GNs are capable of hosting AAAB molecules in the lipophilic central cavity of β-CD. UV−vis spectra are applied to prove the inclusion of AAAB with CD-GNs.[57] It is well-known that the Azo groups show a characteristic absorption peak at ~350 nm. There is no doubt that single AAAB shows obvious absorption at 357 nm. Figure 3 shows the UV−vis spectra of AAAB solution in the presence

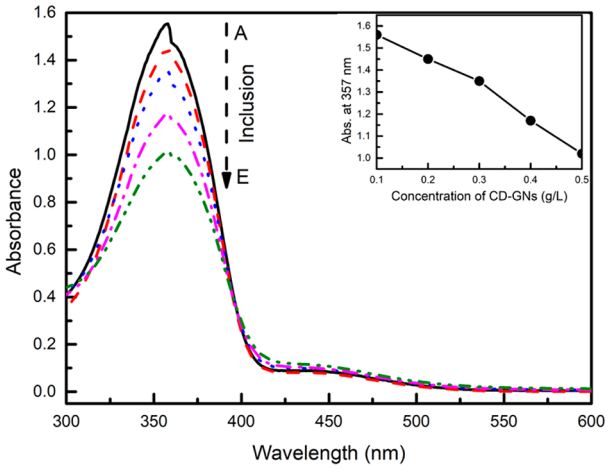

Figure 3. UV−vis spectra of AAAB (25 μM) in the presence of CD-GNs (0.1, 0.2, 0.3, 0.4, and 0.5 g/L from A to E). The inset represents changes in UV−vis absorption of AAAB at 357 nm with different concentrations of CD-GNs.

of CD-GNs. With the increase of the CD-GNs concentration, the absorption peak located at 357 nm decreases gradually. Once the CD-GNs are added into the solution, AAAB immediately enters into the extremely hydrophobic and electron dense β-CD cavity. By adding CD-GNs from 0 to 0.5 g/L, the absorbance at 357 nm decreases linearly with increasing the concentration (Figure 3, inset), indicating the concentration-dependent manner of AAAB inclusion.

The obtained CD-GNs/AAAB complexes are added into the UV-curable epoxy resin system. Because the bisphenol A epoxy

DOI: 10.1021/acs.macromol.8b01124
Macromolecules 2018, 51, 5294−5303

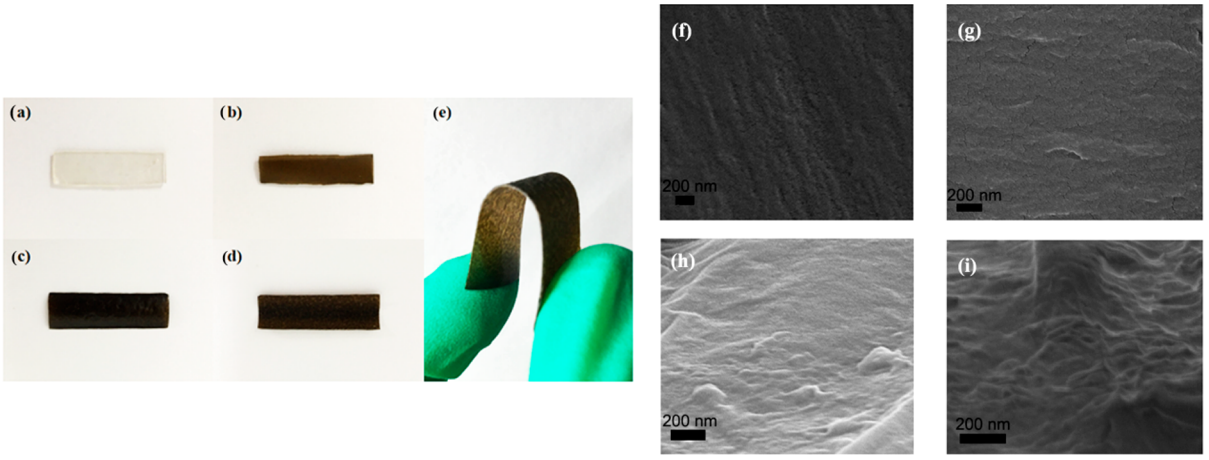

Figure 4. Photographs of epoxy composite films with (a) 0%, (b) 5%, (c) 10%, and (d) 15% CD-GNs/AAAB complexes. (e) Photograph of epoxy composite films under bending state. Representative SEM images of the cross section of the fracture surfaces of epoxy composite films with (f) 0%, (g) 5%, (h) 10%, and (i) 15% CD-GNs/AAAB complexes.

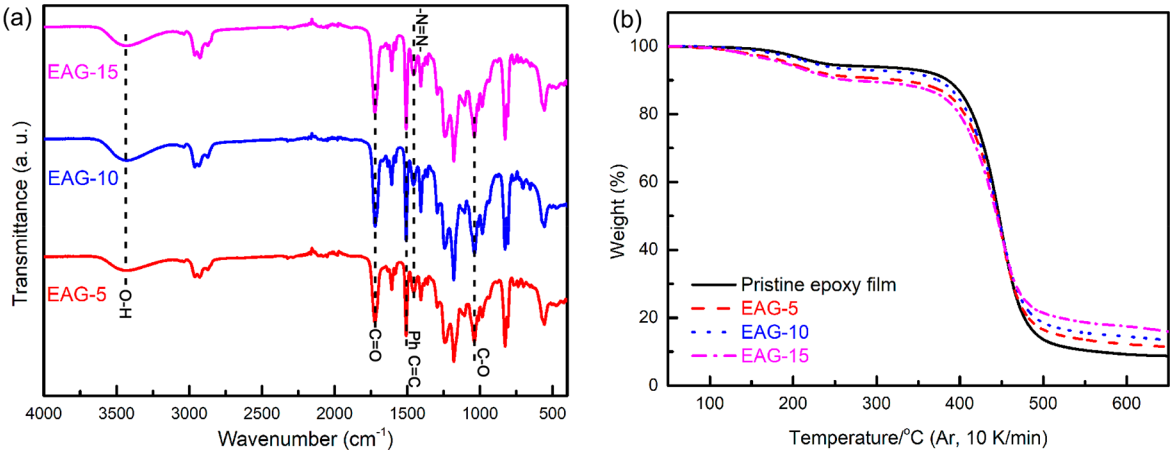

Figure 5. (a) FT-IR spectra of pristine epoxy and EAG composite films. (b) TGA curves of epoxy and EAG composite films in Ar at a heating rate of 10 K/min.

diacrylate has a certain viscosity, these complexes cannot move or dissociate freely. Meanwhile, as the UV curing process is in undisturbed state, the complexes are fixed in their original positions. Subsequently, the UV-curing-induced exclusion between CD-GNs and AAAB would be recombined in the following dark environment. As the AAAB contains C═C bonds, the inclusion complexes can be polymerized with unsaturated epoxy monomers to effectively introduce the multipoint reversible host−guest interactions into 3D cross-linking structure of epoxy resins. The obtained resins are convenient to be endowed with self-healing properties through the association and dissociation of complex linkers with CD-GNs and AAAB moieties. Epoxy composites with CD-GNs/AAAB compositions of 5, 10, and 15 wt % are recorded as EAG-5, EAG-10, and EAG-15, respectively. Figure 4a−e shows the digital photos of epoxy composite films. The scraping process ensures the facile preparation of flexible, smooth, and dark EAG composite films as well as transparent epoxy films. In the present study, the CD-GNs/AAAB complex is first well dispersed in butyl acrylate and then mixed in epoxy acrylate. The mixture is dispersed with the assistance of ultrasonic treatment to ensure the uniform dispersion of the complex. The cross-sectional SEM image of epoxy film represents smooth fracture surface (Figure 4f). Compared with epoxy, the SEM images of EAG composite films represent rougher surface structure (Figure 4g−i). It seems that some parallel substances (much thicker than graphene) are pulled out when the film is cut off. The lamellar bulges are irregularly distributed on the fracture surface, indicating uniform dispersion of graphene in epoxy resin. During the in situ UV curing, the CD-GNs/AAAB complexes are randomly distributed in epoxy resins. As nanomaterials with super large specific surface area, the CD-GNs/AAAB sheets are decorated with long epoxy acrylate chains via copolymerization and $\pi-\pi$ interactions between bisphenol A moieties and graphene. Consequently, the parallel substances on the fracture surfaces of composite films may be the polymer wrapped graphene. These results reveal that the CD-GNs/AAAB is uniformly distributed in epoxy to provide a high density of reversible junctions.

All the FT-IR spectra of epoxy composite films show highly similar features (Figure 5a). The spectra represent the characteristic peaks at ∼3440 cm^{-1} (O−H), 1720 cm^{-1} (C═O of GO and epoxy acrylate), and 1605 and 1508 cm^{-1} (Ph C═C of epoxy), indicating the existence of epoxy acrylate in the films. The results indicate that the chemical structure of epoxy resin is basically unchanged after the in situ curing with CD-GNs/AAAB complex. Moreover, the IR spectra represent the peaks located at ∼1405 cm^{-1} (O−H

DOI: 10.1021/acs.macromol.8b01124
Macromolecules 2018, 51, 5294−5303

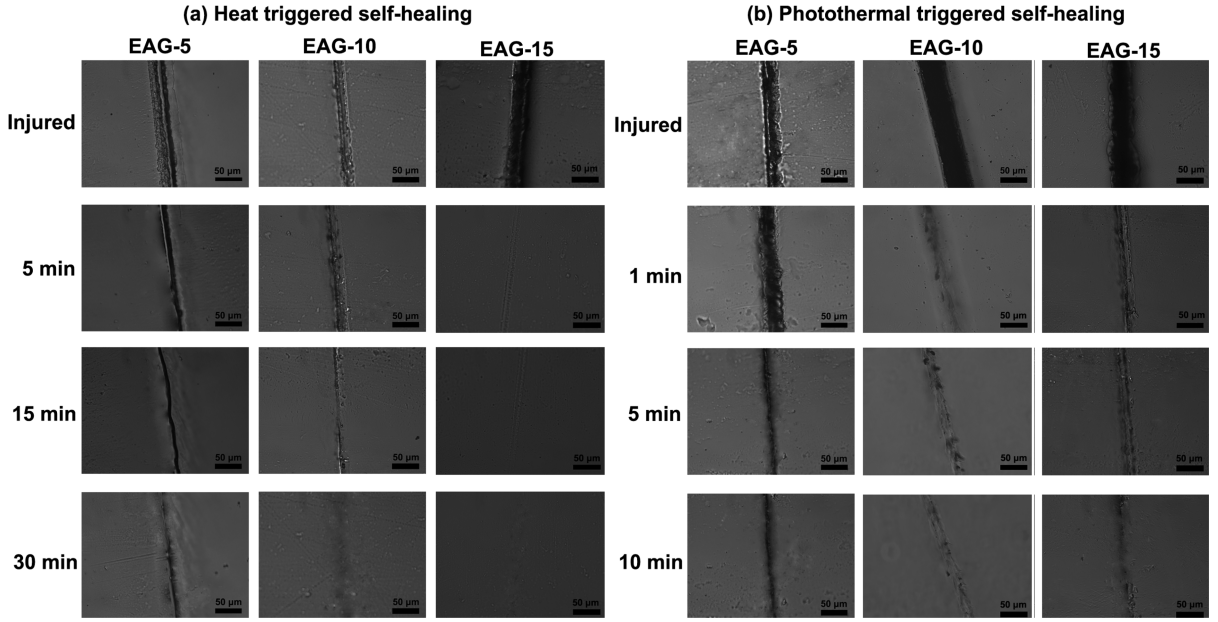

Figure 6. (a) Heating triggered recovery of epoxy composite films under 120 °C detected by an optical microscope. (b) Photothermal effect triggered recovery of epoxy composite films under NIR irradiation (laser power: 2.0 W; vertical distance: 5 cm).

bending vibration of β-CD), 1038 cm^{-1} (C−O absorption of β-CD), and 1457 cm^{-1} (−N═N−), which may be a proof of the existence of the host−guest interactions. As the self-healing behavior is related to thermal stimulus, the thermal stability of epoxy resins is studied by TGA (Figure 5b). All the samples show moderate weight loss between 150 and 375 °C due to the decomposition of oxygen-containing, heat labile groups. Then, the composite films show a sharp weight loss beginning at ~375 °C, which can be attributed to the pyrolysis of epoxy resins. Generally, the presence of CD-GNs/AAAB complexes does not have significant effects on the thermal stability of epoxy. However, as the graphene is carbon-rich molecules, the mass residue of epoxy with different contents of complexes (0, 5, 10, and 15%) at 650 °C is significantly increased from 8.9 to 11.6, 13.7, and 16.1 wt %, respectively. By considering the mass residues of CD-GNs (34.3%) at 650 °C, the amount of CD-GNs in epoxy resin is calculated to be 10.0, 18.8, and 28.3 wt % for EAG-5, EAG-10, and EAG-15, respectively. Although the calculated values are higher that actual adding amount of CD-GNs, both of them present the same linear upward trend.

It is believed that two events are involved in the self-healing process: physical flow of polymer chains at the crack area and recombination of cleaved bonds. This means that the self-healing ability can be achieved by heating the system temperature to above the glass transition temperature (T_g). Figure S6 shows the DMA curves of the epoxy composite films. The T_g of pristine epoxy film is 71.5 °C. In the present study, the graphene can be regarded as macro-cross-linker, which would further increase the cross-linking degree of the composites. With increasing the amount of CD-GNs/AAAB complexes (5, 10, and 15%), the T_g of the composite films gradually increased to 82.4, 87.7, and 88.9 °C, respectively. According to the T_g value, the self-healing temperature was set to 120 °C in this work.

For visual observation of the self-healing process, the epoxy composite films are systematically detected using an optical microscope. The optical photos after 0, 5, 15, and 30 min healing at 120 °C are exhibited in Figure 6a. Crack (~30 μm) is clearly observed on the surface of the injured sample. For all films, only slight traces are remained after healing at 120 °C for 15 min. However, the optimal healing effects could be achieved after 30 min treatment. Furthermore, the composite films show better self-healing effects with the increase of CD-GNs/AAAB content. The destruction and prior UV irradiation of the composite films break the connection of CD-GNs and Azo. This host−guest pair has a greater tendency to link together. The higher the CD-GNs/AAAB content is the more host−guest interactions are at the crack interface, enabling more effective healing effects.

The graphene can in situ transform NIR light into thermal energy to trigger the host−guest interactions.[58,59] Herein, the photothermal triggered self-healing behavior of the epoxy composite films was further examined (Figure 6b). The SEM images prove that the NIR irradiation has comparable healing effects to that of heating. Similarly, the self-healing efficiency of the films increases significantly with the increase of CD-GNs/AAAB content. The photothermal induced temperature elevation curves of the crack surfaces are presented in Figure S7. The temperature of pristine epoxy film only reaches 39.3 °C after 5 min NIR irradiation. For resins containing CD-GNs/AAAB, the temperature increases rapidly and reaches equilibrium in only 100 s. With increasing the concentration of CD-GNs/AAAB (5, 10, and 15%), the maximum temperatures of laser facula increase from 20.0 to 117.2, 125.0, and 139.1 °C, respectively. Both polymer chain movement and reconstruction of host−guest interactions can occur at this high temperature. The SEM results also reveal that the required treatment time of photothermal method to achieve optimal healing effects is significantly reduced (specifically, 30 min for the heating and only 10 min for NIR irradiation). This may be because partial thermal energy is consumed to cause irrelevant molecular chain movement during the transfer process from the heat source to the injury site of films. Meanwhile, the optimal healing effects appear to be worse than heating, as the repaired films still have some small cracks. This phenomenon can be explained as the heating stimulus leads to more uniform

DOI: 10.1021/acs.macromol.8b01124
Macromolecules 2018, 51, 5294−5303

self-healing effects than the NIR irradiation for internal damages of the sample.

The tensile stress−strain curves of the epoxy composite films are shown in Figure 7. The pristine epoxy film exhibits a

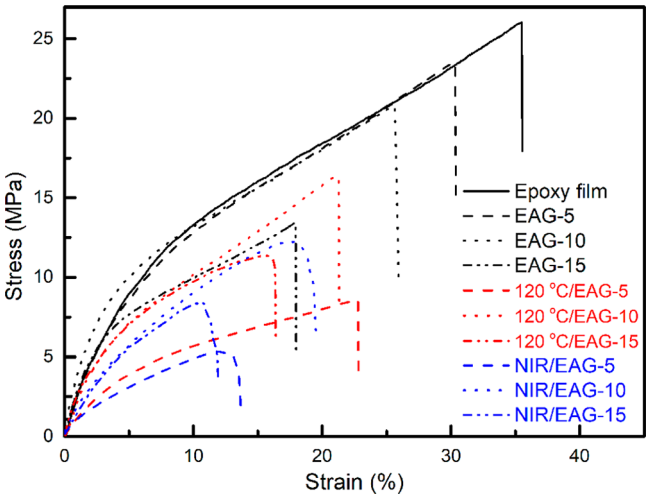

Figure 7. Tensile stress−strain curves of epoxy composite films after healing at 120 °C for 30 min or under NIR irradiation for 15 min.

flexible elongation of 35.4% and a tensile strength of 26.1 MPa. For EAG-5, EAG-10, and EAG-15, the tensile strength decreases to 23.5, 20.8, and 13.5 MPa, respectively. This is because the high content of graphene will reduce the mechanical strength of the composites. In present study, the ratio of healed tensile strength to original tensile strength is used to quantitatively evaluate the self-healing efficiency. Table 1 clearly reveals that the self-healing efficiency of the films increases with the increase of CD-GNs/AAAB content. These results suggest that relatively low CD-GNs/AAAB contents (less than 5%) are not enough to produce sufficient host−guest interactions for the self-healing. As shown in Table 1, the healing efficiencies increase rapidly within the first 15 min and then flatten in continuous 120 °C heating treatment, suggesting that the self-healing gradually reaches optimization in 30 min. Similar trends are observed in the photothermal triggered self-healing process. However, the recovery speed of photothermal method to achieve optimal healing effects is faster than heating, which is in accordance with the results obtained by optical microscope. It is worth noting that the EAG-10 has the maximum recovered tensile strength (16.5 MPa) after healing at 120 °C for 30 min. Although the EAG-15 possesses more host−guest pairs and better healing efficiencies, the poor initial strength of EAG-15 (only 13.5 MPa) eventually leads to a lower healed strength of the composite. The repetitive healing performances of epoxy composites are also investigated. The EAG-10 exhibits excellent healing in up to four cycles. The strength recovery rates of heat or photothermal triggered self-healing are 68.8% and 38.9% after four cycles of repair, respectively (Figure S8).

Since there are several previous works that report the self-healing behaviors of epoxy resin and host−guest systems,[37−41,60−66] herein, the current results were compared with others for a more comprehensive evaluation. Plotting the data collected from the references show that the present EAG composite films possess the highest tensile strength among other host−guest interaction systems (most of them are hydrogels) (Figure 8). Compared with other intrinsic self-

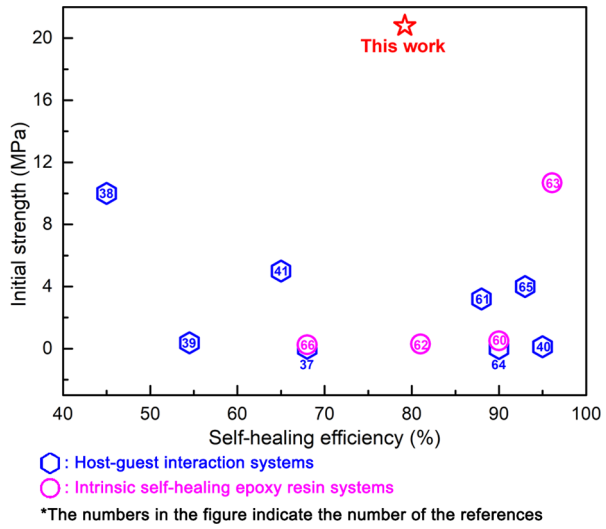

Figure 8. Comparisons of self-healing efficiency and initial strength with epoxy resin and host−guest systems.

healing epoxy resin systems, our EAG composite films also show the highest initial strength and relatively high healing efficiency. As shown in Figure 9, the external damage breaks

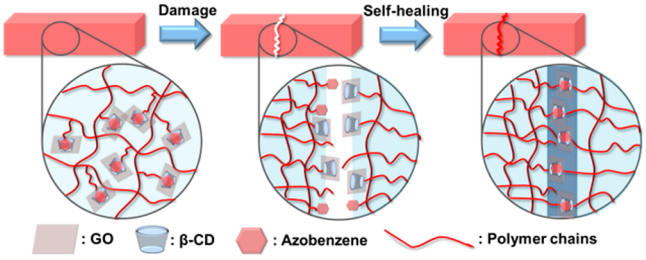

Figure 9. Schematic illustration of the self-healing mechanism of epoxy composite films.

the connection between β-CD (host, CD-GNs moieties) and azobenzene (guest, AAAB moieties). Prior to the self-healing process, the damaged samples are irradiated by 365 nm UV

Table 1. Heating or Photothermal Effect Triggered Self-Healing Efficiencies of the Epoxy Composite Films for Different Times

	self-healing efficiencies (%)/recovered tensile stress (MPa)					
	heating (120 °C)			photothermal effect (NIR, 2 W)		
samples	5 min	15 min	30 min	1 min	5 min	10 min
EAG-5	17.3/4.1	33.4/7.8	37.0/8.7	−/−	18.9/4.4	23.1/5.4
EAG-10	33.1/6.9	70.5/14.7	79.2/16.5	22.6/4.7	52.8/11.0	59.4/12.4
EAG-15	45.3/6.1	73.2/9.9	85.1/11.5	29.4/4.0	55.3/7.5	63.4/8.6

DOI: 10.1021/acs.macromol.8b01124
Macromolecules 2018, 51, 5294−5303

light to disconnect the connection between the host and guest molecules. This step increases both the amount of combinative host−guest moieties and the epoxy chain mobility on the damage sites, which would improve the self-healing efficiency. These host−guest moieties are "eager" to re-form the cross-linking of epoxy and graphene, endowing resins with good mechanical properties and intrinsic self-healing ability. It should be noted that the achievement of excellent self-healing behaviors triggered by facile multistimuli (heat or NIR) can be very helpful for fabricating novel self-healing epoxy resins for practical applications. As many other functional polymers or particles could be also easily modified by CDs, it is worth noting that the present strategy can also introduce various sorts of cross-linking structure containing polymers or nanoparticles, which should be valuable for developing smart materials with multiple functions such as electromagnetic wave absorption,[67,68] sensing,[69−71] environmental remediation,[72−77] and healing properties.

4. CONCLUSIONS

In the present study, intrinsic self-healing epoxy resin was fabricated via novel graphene-assisted host−guest chemistry. The CD-GNs/AAAB, acting as macro-cross-linker and photothermal agent, was prepared by attaching the β-CD to graphene via amidation, followed by the inclusion of AAAB through the host−guest interactions. CD-GNs/AAAB was readily blended with unsaturated epoxy resin via the UV-curing process to fabricate EAG composite films. In order to achieve physical flow of epoxy chains at the crack area, heating or NIR was used to trigger the self-healing process. Benefiting from the cross-linked anchoring effects of graphene, the cleaved bonds are recombined through the inclusion of CD-GNs on AAAB. Self-healing property measurements reveal that the EAG-10 films exhibit excellent tensile strength (20.8 MPa) and healing efficiency (79.2%). The present host−guest macro-cross-linking strategy endows the traditional epoxy resin with outstanding mechanical and self-healing properties, promoting the practical application of smart materials in engineering. Moreover, considering that the graphene can be replaced by other nanomaterials, such as carbon nanotubes, metallic oxide, ceramics, and quantum dots, multiple functions with spontaneously healing properties are expected to be prepared via the present strategy.

■ ASSOCIATED CONTENT

Supporting Information

The Supporting Information is available free of charge on the ACS Publications website at DOI: 10.1021/acs.macromol.8b01124.

Figure S1: FT-IR, ^{1}H NMR, and ^{13}C NMR spectra of AAAB; Figure S2: FT-IR, ^{1}H NMR, and ^{13}C NMR spectra of 6-OTs-β-CD; Figure S3: FT-IR, ^{1}H NMR, and ^{13}C NMR spectra of 6-NH_2-β-CD; Figure S4: XPS spectra of GO and CD-GNs; Figure S5: the dispersion photos of GO and CD-GNs; Figure S6: DMA curves of pristine epoxy and EAG composite films; Figure S7: temperature elevation of the crack surfaces of composite films; Figure S8: tensile stress after multiple cycles of damage and healing (PDF)

■ AUTHOR INFORMATION

Corresponding Authors

*E-mail: huzhen@hit.edu.cn (Z.H.).
*E-mail: zguo10@utk.edu (Z.G.).
*E-mail: yudonghuang@163.com (Y.H.).

ORCID

Zhen Hu: 0000-0002-0160-782X
Hu Liu: 0000-0003-3840-8135
Zhanhu Guo: 0000-0003-0134-0210

Notes

The authors declare no competing financial interest.

■ ACKNOWLEDGMENTS

We thank the National Natural Science Foundation of China (no. 51673053), the Natural Science Foundation of Heilongjiang Province (no. LC2017024), and the Fundamental Research Funds for the Central Universities (no. HIT. IBRSEM. 2013016).

■ REFERENCES

(1) Yang, Y.; Ding, X.; Urban, M. W. Chemical and Physical Aspects of Self-healing Materials. *Prog. Polym. Sci.* **2015**, *49−50*, 34−59.
(2) Yang, Y.; Urban, M. W. Self-healing Polymeric Materials. *Chem. Soc. Rev.* **2013**, *42*, 7446−67.
(3) Yan, X.; Xu, D.; Chi, X.; Chen, J.; Dong, S.; Ding, X.; Yu, Y.; Huang, F. A Multiresponsive, Shape-persistent, and Elastic Supramolecular Polymer Network Gel Constructed by Orthogonal Self-assembly. *Adv. Mater.* **2012**, *24*, 362−9.
(4) Ji, X.; Shi, B.; Wang, H.; Xia, D.; Jie, K.; Wu, Z. L.; Huang, F. Supramolecular Construction of Multifluorescent Gels: Interfacial Assembly of Discrete Fluorescent Gels through Multiple Hydrogen Bonding. *Adv. Mater.* **2015**, *27*, 8062−6.
(5) Ji, X.; Xia, D.; Yan, X.; Wang, H.; Huang, F. Supramolecular Polymer Materials Based on Crown Ether and Pillararene Host-Guest Recognition Motifs. *Acta Polym. Sin.* **2017**, *1*, 9−18.
(6) Gao, L.; He, J.; Hu, J.; Wang, C. Photoresponsive Self-Healing Polymer Composite with Photoabsorbing Hybrid Microcapsules. *ACS Appl. Mater. Interfaces* **2015**, *7*, 25546−52.
(7) Guo, W.; Jia, Y.; Tian, K.; Xu, Z.; Jiao, J.; Li, R.; Wu, Y.; Cao, L.; Wang, H. UV-Triggered Self-Healing of a Single Robust SiO_2Microcapsule Based on Cationic Polymerization for Potential Application in Aerospace Coatings. *ACS Appl. Mater. Interfaces* **2016**, *8*, 21046−54.
(8) Hillewaere, X. K. D.; Teixeira, R. F. A.; Nguyen, L.-T. T.; Ramos, J. A.; Rahier, H.; Du Prez, F. E. Autonomous Self-Healing of Epoxy Thermosets with Thiol-Isocyanate Chemistry. *Adv. Funct. Mater.* **2014**, *24*, 5575−83.
(9) Jin, H.; Mangun, C. L.; Stradley, D. S.; Moore, J. S.; Sottos, N. R.; White, S. R. Self-healing Thermoset Using Encapsulated Epoxy-amine Healing Chemistry. *Polymer* **2012**, *53*, 581−7.
(10) Yuan, Y. C.; Ye, X. J.; Rong, M. Z.; Zhang, M. Q.; Yang, G. C.; Zhao, J. Q. Self-healing Epoxy Composite with Heat-resistant Healant. *ACS Appl. Mater. Interfaces* **2011**, *3*, 4487−95.
(11) Hart, K. R.; Sottos, N. R.; White, S. R. Repeatable Self-healing of an Epoxy Matrix Using Imidazole Initiated Polymerization. *Polymer* **2015**, *67*, 174−84.
(12) Luterbacher, R.; Trask, R. S.; Bond, I. P. Static and Fatigue Tensile Properties of Cross-ply laminates Containing Vascules for Self-healing Applications. *Smart Mater. Struct.* **2016**, *25*, 015003.
(13) Bai, N.; Saito, K.; Simon, G. P. Synthesis of a Diamine Cross-linker Containing Diels−Alder Adducts to Produce Self-healing Thermosetting Epoxy Polymer from a Widely Used Epoxy Monomer. *Polym. Chem.* **2013**, *4*, 724−30.
(14) Kuang, X.; Liu, G.; Dong, X.; Liu, X.; Xu, J.; Wang, D. Facile Fabrication of Fast Recyclable and Multiple Self-healing Epoxy

DOI: 10.1021/acs.macromol.8b01124
Macromolecules 2018, 51, 5294−5303

Materials through Diels-Alder Adduct Cross-linker. *J. Polym. Sci., Part A: Polym. Chem.* **2015**, *53*, 2094−103.
(15) Chen, X.; Dam, M. A.; Ono, K.; Mal, A.; Shen, H.; Nutt, S. R.; Sheran, K.; Wudl, F. A Thermally Re-mendable Cross-Linked Polymeric Material. *Science* **2002**, *295*, 1698−1702.
(16) Min, Y.; Huang, S.; Wang, Y.; Zhang, Z.; Du, B.; Zhang, X.; Fan, Z. Sonochemical Transformation of Epoxy−Amine Thermoset into Soluble and Reusable Polymers. *Macromolecules* **2015**, *48*, 316−22.
(17) Tian, Q.; Yuan, Y. C.; Rong, M. Z.; Zhang, M. Q. A thermally remendable epoxy resin. *J. Mater. Chem.* **2009**, *19*, 1289−96.
(18) Zhang, J.; Niu, Y.; Huang, C.; Xiao, L.; Chen, Z.; Yang, K.; Wang, Y. Self-healable and Recyclable Triple-shape PPDO−PTMEG Co-network Constructed through Thermoreversible Diels−Alder Reaction. *Polym. Chem.* **2012**, *3*, 1390−3.
(19) Hernández, M.; Grande, A. M.; Dierkes, W.; Bijleveld, J.; van der Zwaag, S.; García, S. J. Turning Vulcanized Natural Rubber into a Self-Healing Polymer: Effect of the Disulfide/Polysulfide Ratio. *ACS Sustainable Chem. Eng.* **2016**, *4*, 5776−84.
(20) Lafont, U.; van Zeijl, H.; van der Zwaag, S. Influence of Cross-linkers on the Cohesive and Adhesive Self-healing Ability of Polysulfide-based Thermosets. *ACS Appl. Mater. Interfaces* **2012**, *4*, 6280−8.
(21) Lei, Z. Q.; Xiang, H. P.; Yuan, Y. J.; Rong, M. Z.; Zhang, M. Q. Room-Temperature Self-Healable and Remoldable Cross-linked Polymer Based on the Dynamic Exchange of Disulfide Bonds. *Chem. Mater.* **2014**, *26*, 2038−46.
(22) Altuna, F. I.; Pettarin, V.; Williams, R. J. J. Self-healable Polymer Networks Based on the Cross-linking of Epoxidised Soybean Oil by an Aqueous Citric Acid Solution. *Green Chem.* **2013**, *15*, 3360.
(23) Ghazi, A.; Ghasemi, E.; Mahdavian, M.; Ramezanzadeh, B.; Rostami, M. The Application of Benzimidazole and Zinc Cations Intercalated Sodium Montmorillonite as Smart Ion Exchange Inhibiting Pigments in the Epoxy Ester Coating. *Corros. Sci.* **2015**, *94*, 207−217.
(24) Long, R.; Qi, H. J.; Dunn, M. L. Modeling the Mechanics of Covalently Adaptable Polymer Networks with Temperature-dependent Bond Exchange Reactions. *Soft Matter* **2013**, *9*, 4083.
(25) Chen, Y.; Guan, Z. Multivalent Hydrogen Bonding Block Copolymers Self-assemble into Strong and Tough Self-healing Materials. *Chem. Commun.* **2014**, *50*, 10868−70.
(26) Cordier, P.; Tournilhac, F.; Soulié-Ziakovic, C.; Leibler, L. Self-healing and Thermoreversible Rubber from Supramolecular Assembly. *Nature* **2008**, *451*, 977−80.
(27) Hentschel, J.; Kushner, A. M.; Ziller, J.; Guan, Z. Self-healing Supramolecular Block Copolymers. *Angew. Chem., Int. Ed.* **2012**, *51*, 10561−5.
(28) Hart, L. R.; Harries, J. L.; Greenland, B. W.; Colquhoun, H. M.; Hayes, W. Healable Supramolecular Polymers. *Polym. Chem.* **2013**, *4*, 4860−70.
(29) Vaiyapuri, R.; Greenland, B. W.; Colquhoun, H. M.; Elliott, J. M.; Hayes, W. Molecular Recognition between Functionalized Gold Nanoparticles and Healable, Supramolecular Polymer Blends − a Route to Property Enhancement. *Polym. Chem.* **2013**, *4*, 4902−9.
(30) Basak, S.; Nanda, J.; Banerjee, A. Multi-stimuli Responsive Self-healing Metallo-Hydrogels: Tuning of the Gel Recovery Property. *Chem. Commun.* **2014**, *50*, 2356−9.
(31) Wang, Z.; Fan, W.; Tong, R.; Lu, X.; Xia, H. Thermal-healable and Shape Memory Metallosupramolecular Poly(n-butyl acrylate-co-methyl methacrylate) Materials. *RSC Adv.* **2014**, *4*, 25486−93.
(32) Nakahata, M.; Takashima, Y.; Yamaguchi, H.; Harada, A. Redox-responsive Self-healing Materials Formed from Host-guest Polymers. *Nat. Commun.* **2011**, *2*, 511−6.
(33) Yan, Q.; Feng, A.; Zhang, H.; Yin, Y.; Yuan, J. Redox-switchable Supramolecular Polymers for Responsive Self-healing Nanofibers in Water. *Polym. Chem.* **2013**, *4*, 1216−20.
(34) Wang, Y.-F.; Zhang, D.-L.; Zhou, T.; Zhang, H.-S.; Zhang, W.-Z.; Luo, L.; Zhang, A.-M.; Li, B.-J.; Zhang, S. A Reversible Functional Supramolecular Material Formed by Host−guest Inclusion. *Polym. Chem.* **2014**, *5*, 2922−7.
(35) Chuo, T.-W.; Wei, T.-C.; Liu, Y.-L. Electrically Driven Self-healing Polymers Based on Reversible Guest-host Complexation of β-cyclodextrin and Ferrocene. *J. Polym. Sci., Part A: Polym. Chem.* **2013**, *51*, 3395−403.
(36) Kakuta, T.; Takashima, Y.; Nakahata, M.; Otsubo, M.; Yamaguchi, H.; Harada, A. Preorganized Hydrogel: Self-healing Properties of Supramolecular Hydrogels Formed by Polymerization of Host-guest-Monomers that Contain Cyclodextrins and Hydrophobic Guest Groups. *Adv. Mater.* **2013**, *25*, 2849−53.
(37) Miyamae, K.; Nakahata, M.; Takashima, Y.; Harada, A. Self-Healing, Expansion-Contraction, and Shape-Memory Properties of a Preorganized Supramolecular Hydrogel through Host-Guest Interactions. *Angew. Chem., Int. Ed.* **2015**, *54*, 8984−7.
(38) Nakahata, M.; Takashima, Y.; Harada, A. Highly Flexible, Tough, and Self-Healing Supramolecular Polymeric Materials Using Host-Guest Interaction. *Macromol. Rapid Commun.* **2016**, *37*, 86−92.
(39) Guo, K.; Zhang, D. L.; Zhang, X. M.; Zhang, J.; Ding, L. S.; Li, B. J.; Zhang, S. Conductive Elastomers with Autonomic Self-healing Properties. *Angew. Chem., Int. Ed.* **2015**, *54*, 12127−33.
(40) Yu, C.; Wang, C.-F.; Chen, S. Robust Self-Healing Host-Guest Gels from Magnetocaloric Radical Polymerization. *Adv. Funct. Mater.* **2014**, *24*, 1235−42.
(41) Takashima, Y.; Yonekura, K.; Koyanagi, K.; Iwaso, K.; Nakahata, M.; Yamaguchi, H.; Harada, A. Multifunctional Stimuli-Responsive Supramolecular Materials with Stretching, Coloring, and Self-Healing Properties Functionalized via Host−Guest Interactions. *Macromolecules* **2017**, *50*, 4144−50.
(42) Hu, Z.; Wang, C.; Zhao, F.; Xu, X.; Wang, S.; Yu, L.; Zhang, D.; Huang, Y. Fabrication of a Graphene/C_{60} Nanohybrid via Gamma-cyclodextrin Host-guest Chemistry for Photodynamic and Photothermal Therapy. *Nanoscale* **2017**, *9*, 8825−33.
(43) Hu, Z.; Zhang, D.; Yu, L.; Huang, Y. Light-triggered C60 Release from a Graphene/cyclodextrin Nanoplatform for the Protection of Cytotoxicity Induced by Nitric Oxide. *J. Mater. Chem. B* **2018**, *6*, 518−26.
(44) Rekharsky, M. V.; Inoue, Y. Complexation Thermodynamics of Cyclodextrins. *Chem. Rev.* **1998**, *98*, 1875−1917.
(45) Chen, H.; Ma, X.; Wu, S.; Tian, H. A Rapidly Self-healing Supramolecular Polymer Hydrogel with Photostimulated Room-temperature Phosphorescence Responsiveness. *Angew. Chem., Int. Ed.* **2014**, *53*, 14149−52.
(46) Hu, Z.; Shao, Q.; Huang, Y.; Yu, L.; Zhang, D.; Xu, X.; Lin, J.; Liu, H.; Guo, Z. Light Triggered Interfacial Damage Self-healing of Poly(p-phenylene benzobisoxazole) Fiber Composites. *Nanotechnology* **2018**, *29*, 185602.
(47) Shao, Q.; Hu, Z.; Xu, X.; Yu, L.; Zhang, D.; Huang, Y. Mussel-inspired Immobilization of BN Nanosheets onto Poly(p-phenylene benzobisoxazole) Fibers: Multifunctional Interface for Photothermal Self-healing. *Appl. Surf. Sci.* **2018**, *440*, 1159−65.
(48) Hu, Z.; Shao, Q.; Moloney, M. G.; Xu, X.; Zhang, D.; Li, J.; Zhang, C.; Huang, Y. Nondestructive Functionalization of Graphene by Surface-Initiated Atom Transfer Radical Polymerization: An Ideal Nanofiller for Poly(p-phenylene benzobisoxazole) Fibers. *Macromolecules* **2017**, *50*, 1422−9.
(49) Hu, Z.; Shao, Q.; Xu, X.; Zhang, D.; Huang, Y. Surface Initiated Grafting of Polymer Chains on Carbon Nanotubes via One-step Cycloaddition of Diarylcarbene. *Compos. Sci. Technol.* **2017**, *142*, 294−301.
(50) Hu, Z.; Song, C.; Shao, Q.; Li, J.; Huang, Y. One-step Functionalization of Graphene by Cycloaddition of Diarylcarbene and Its Application as Reinforcement in Epoxy Composites. *Compos. Sci. Technol.* **2016**, *135*, 21−7.
(51) Guo, Y.; Xu, G.; Yang, X.; Ruan, K.; Ma, T.; Zhang, Q.; Gu, J.; Wu, Y.; Liu, H.; Guo, Z. Significantly Enhanced and Precisely Modeled Thermal Conductivity in Polyimide Nanocomposites with Chemically Modified Graphene via in situ Polymerization and

DOI: 10.1021/acs.macromol.8b01124
Macromolecules 2018, 51, 5294−5303

Electrospinning-hot Press Technology. *J. Mater. Chem. C* **2018**, *6*, 3004−15.
(52) Guo, Y.; Guo, S.; Ren, J.; Zhai, Y.; Dong, S.; Wang, E. Cyclodextrin Functionalized Graphene Nanosheets with High Supramolecular Recognition Capability: Synthesis and Host-Guest Inclusion for Enhanced Electrochemical Performance. *ACS Nano* **2010**, *4*, 4001−10.
(53) Guan, X.; Zheng, G.; Dai, K.; Liu, C.; Yan, X.; Shen, C.; Guo, Z. Carbon Nanotubes-Adsorbed Electrospun PA66 Nanofiber Bundles with Improved Conductivity and Robust Flexibility. *ACS Appl. Mater. Interfaces* **2016**, *8*, 14150−9.
(54) Wu, Z.; Cui, H.; Chen, L.; Jiang, D.; Weng, L.; Ma, Y.; Li, X.; Zhang, X.; Liu, H.; Wang, N.; Zhang, J.; Ma, Y.; Zhang, M.; Huang, Y.; Guo, Z. Interfacially Reinforced Unsaturated Polyester Carbon Fiber Composites with a Winyl Ester-carbon Nanotubes Sizing Agent. *Compos. Sci. Technol.* **2018**, *164*, 195−203.
(55) Hu, C.; Li, Z.; Wang, Y.; Gao, J.; Dai, K.; Zheng, G.; Liu, C.; Shen, C.; Song, H.; Guo, Z. Comparative Assessment of the Strain-sensing Behaviors of Polylactic Acid Nanocomposites: Reduced Graphene Oxide or Carbon Nanotubes. *J. Mater. Chem. C* **2017**, *5*, 2318−28.
(56) Sun, K.; Xie, P.; Wang, Z.; Su, T.; Shao, Q.; Ryu, J.; Zhang, X.; Guo, J.; Shankar, A.; Li, J.; Fan, R.; Cao, D.; Guo, Z. Flexible Polydimethylsiloxane/Multi-walled Carbon Nanotubes Membranous Metacomposites with Negative Permittivity. *Polymer* **2017**, *125*, 50−7.
(57) Li, J.; Zhou, Z.; Ma, L.; Chen, G.; Li, Q. Hierarchical Assembly of Amphiphilic POSS-Cyclodextrin Molecules and Azobenzene End-Capped Polymers. *Macromolecules* **2014**, *47*, 5739−48.
(58) Hu, Z.; Zhao, F.; Wang, Y.; Huang, Y.; Chen, L.; Li, N.; Li, J.; Li, Z.; Yi, G. Facile Fabrication of a C60-Polydopamine-Graphene Nanohybrid for Single Light Induced Photothermal and Photodynamic Therapy. *Chem. Commun.* **2014**, *50*, 10815−8.
(59) Hu, Z.; Li, J.; Huang, Y.; Chen, L.; Li, Z. Functionalized Graphene/C60 Nanohybrid for Targeting Photothermally Enhanced Photodynamic Therapy. *RSC Adv.* **2015**, *5*, 654−64.
(60) Canadell, J.; Goossens, H.; Klumperman, B. Self-Healing Materials Based on Disulfide Links. *Macromolecules* **2011**, *44*, 2536−41.
(61) Kakuta, T.; Takashima, Y.; Sano, T.; Nakamura, T.; Kobayashi, Y.; Yamaguchi, H.; Harada, A. Adhesion between Semihard Polymer Materials Containing Cyclodextrin and Adamantane Based on Host−Guest Interactions. *Macromolecules* **2015**, *48*, 732−38.
(62) Pepels, M.; Filot, I.; Klumperman, B.; Goossens, H. Self-healing Systems Based on Disulfide−thiol Exchange Reactions. *Polym. Chem.* **2013**, *4*, 4955−65.
(63) Tian, Q.; Rong, M. Z.; Zhang, M. Q.; Yuan, Y. C. Synthesis and Characterization of Epoxy with Improved Thermal Remendability Based on Diels-Alder Reaction. *Polym. Int.* **2010**, *59*, 1339−45.
(64) Yang, Q.; Wang, P.; Zhao, C.; Wang, W.; Yang, J.; Liu, Q. Light-Switchable Self-Healing Hydrogel Based on Host-Guest Macro-Crosslinking. *Macromol. Rapid Commun.* **2017**, *38*, 1600741−7.
(65) Zhang, D. L.; Ju, X.; Li, L. H.; Kang, Y.; Gong, X. L.; Li, B. J.; Zhang, S. An Efficient Multiple Healing Conductive Composite via Host-guest Inclusion. *Chem. Commun.* **2015**, *51*, 6377−80.
(66) Zhang, Z. P.; Rong, M. Z.; Zhang, M. Q. Room Temperature Self-healable Epoxy Elastomer with Reversible Alkoxyamines as Crosslinkages. *Polymer* **2014**, *55*, 3936−43.
(67) Zhang, K.; Li, G.-H.; Feng, L.-M.; Wang, N.; Guo, J.; Sun, K.; Yu, K.-X.; Zeng, J.-B.; Li, T.; Guo, Z.; Wang, M. Ultralow Percolation Threshold and Enhanced Electromagnetic Interference Shielding in Poly(l-lactide)/Multi-walled Carbon Nanotube Nanocomposites with Electrically Conductive Segregated Networks. *J. Mater. Chem. C* **2017**, *5*, 9359−69.
(68) Guo, Z.; Xie, P.; Dang, F.; He, B.; Lin, J.; Fan, R.; Hou, C.; Liu, H.; Zhang, J.-x.; Ma, Y. Bio-gel Derived Nickel/Carbon Nanocomposites with Enhanced Microwave Absorption. *J. Mater. Chem. C* **2018**, DOI: 10.1039/C8TC02127A.
(69) Liu, H.; Huang, W.; Yang, X.; Dai, K.; Zheng, G.; Liu, C.; Shen, C.; Yan, X.; Guo, J.; Guo, Z. Organic Vapor Sensing Behaviors of Conductive Thermoplastic Polyurethane−Graphene Nanocomposites. *J. Mater. Chem. C* **2016**, *4*, 4459−69.
(70) Gu, H.; Zhang, H.; Lin, J.; Shao, Q.; Young, D. P.; Sun, L.; Shen, T. D.; Guo, Z. Large Negative Giant Magnetoresistance at Room Temperature and Electrical Transport in Cobalt Ferrite-Polyaniline Nanocomposites. *Polymer* **2018**, *143*, 324−30.
(71) Li, Y.; Zhou, B.; Zheng, G.; Liu, X.; Li, T.; Yan, C.; Cheng, C.; Dai, K.; Liu, C.; Shen, C.; Guo, Z. Continuously Prepared Highly Conductive and Stretchable SWNT/MWNT Synergistically Composited Electrospun Thermoplastic Polyurethane Yarns for Wearable Sensing. *J. Mater. Chem. C* **2018**, *6*, 2258−69.
(72) Ma, Y.; Lv, L.; Guo, Y.; Fu, Y.; Shao, Q.; Wu, T.; Guo, S.; Sun, K.; Guo, X.; Wujcik, E. K.; Guo, Z. Porous Lignin Based Poly (acrylic acid)/Organo-montmorillonite Nanocomposites: Swelling Behaviors and Rapid Removal of Pb (II) Ions. *Polymer* **2017**, *128*, 12−23.
(73) Kang, H.; Cheng, Z.; Lai, H.; Ma, H.; Liu, Y.; Mai, X.; Wang, Y.; Shao, Q.; Xiang, L.; Guo, X.; Guo, Z. Superlyophobic Anti-corrosive and Self-cleaning Titania Robust Mesh Membrane with Enhanced Oil/Water Separation. *Sep. Purif. Technol.* **2018**, *201*, 193−204.
(74) Sun, S.; Zhu, L.; Liu, X.; Wu, L.; Dai, K.; Liu, C.; Shen, C.; Guo, X.; Zheng, G.; Guo, Z. Superhydrophobic Shish-kebab Membrane with Self-cleaning and Oil/Water Separation Properties. *ACS Sustainable Chem. Eng.* **2018**, DOI: 10.1021/acssuschemeng.8b01047.
(75) Wang, Y. P.; Zhou, P.; Luo, S. Z.; Liao, X. P.; Wang, B.; Shao, Q.; Guo, X.; Guo, Z. Controllable Synthesis of Monolayer Poly(acrylic acid) on the Channel Surface of Mesoporous Alumina for Pb(II) Adsorption. *Langmuir* **2018**, DOI: 10.1021/acs.langmuir.8b00789.
(76) Wang, Y.-P.; Zhou, P.; Luo, S.-Z.; Guo, S.; Lin, J.; Shao, Q.; Guo, X.; Liu, Z.; Shen, J.; Wang, B.; Guo, Z. In situ Polymerized Poly(acrylic acid)/Alumina Nanocomposites for Pb^{2+} Adsorption. *Adv. Polym. Technol.* **2018**, DOI: 10.1002/adv.21969.
(77) Zhang, Y.; Zhao, M.; Zhang, J.; Shao, Q.; Li, J.; Li, H.; Lin, B.; Yu, M.; Chen, S.; Guo, Z. Excellent Corrosion Protection Performance of Epoxy Composite Coatings Filled with Silane Functionalized Silicon Nitride. *J. Polym. Res.* **2018**, *25*, 130.

DOI: 10.1021/acs.macromol.8b01124
Macromolecules 2018, 51, 5294−5303